Journal of Nuclear Materials 384 (2009) 96–102

Contents lists available at ScienceDirect

Journal of Nuclear Materials

journal homepage: www.elsevier.com/locate/jnucmat

Atomic scale analysis and phase separation understanding in a thermally aged Fe–20 at.%Cr alloy

S. Novy, P. Pareige, C. Pareige *

Groupe de Physique des Matériaux, ERT n°1000, Université et INSA de Rouen, UMR 6634 Avenue de l'Université BP 12, 76801 Saint Etienne du Rouvray, France

ARTICLE INFO

Article history:
Received 6 June 2008
Accepted 21 October 2008

PACS:
81.40.Cd
64.75.Nx
81.30.Bx

ABSTRACT

Fe–Cr model alloys are of interest for understanding of phase separation in structural material for fusion or fission reactors. This motivated the quantitative study of the phase separation in a thermally aged (773 K) Fe–20 at.%Cr alloy using a Tomographic Atom Probe. It is shown that the chromium content in the α' phase evolves with ageing time synonymous of a non-classical nucleation mechanism. The overlap of the nucleation and coarsening regimes is observed. A non-steady coarsening regime occurs before 1067 h of ageing. The solubility limit at 773 K is found to be 14 at.%. A maximum concentration of (83 ± 1) at.% is observed for the Cr-concentration in α' precipitates.

1. Introduction

High-Cr ferritic-martensitic steels of technological interest for structural components of fusion or fission nuclear reactors contain, in most cases, about 9%Cr. In the case of nano-particle dispersion strengthened steels (such as oxides dispersion strengthened steels, for example) the chromium concentration may be higher (14% or even more). Their response to extreme conditions (high temperature, irradiation at the origin of swelling and corrosion) is partly determined by α/α' phase separation. Thus, in the last few years the binary Fe–Cr model alloys have been at the centre of a large amount of basic research, including specific experimental investigations. In particular, recent works address the problem of the numerical simulation of phase separation in this binary alloys, using Atomic Kinetic Monte Carlo tools [1,2]. Also, ab initio calculations and empirical potentials have been used to give new or more realistic physical parameters needed for simulation [3–4]. Quite often, experimental results or data are missing for evaluation or calibration of these models. In the present work, we report the study at the atomic scale, using the Tomographic Atom Probe (TAP), of an iron/high-chromium (20 at.%) model alloy. This highly concentrated alloy was chosen in order to be deep in the miscibility gap of the Fe–Cr phase diagram (almost near the spinodal domain) and the temperature was 773 K in order to have a faster kinetic (for experimental realisation). The Tomographic Atom Probe is a unique instrument giving accurate results on the evolution of the phase composition, size, morphology and number density which are not accessible with global experimental technique such as electrical resistivity, thermo-electrical power or even small angle neutron scattering. Thus, such results are very useful for simulation workers.

The first part of the paper gives details on the material (elaboration and ageing condition) and the atom probe technique (experimental condition) that were used. An exhaustive description of microstructures of the materials aged for different times is reported in the second part. A discussion on the phase separation mechanism, as a consequence of the obtained experimental data, as well as a comparison with results taken from the literature, are summarised in the last part.

2. Material and experimental technique

2.1. Material

The Fe–20 at.%Cr model alloy that was used in this study was cast by electromagnetic field at the Centre d'Etudes de Chimie Métallurgique (CNRS Vitry – France). Samples have been prepared from Atomiron iron 99.98% with 0.005% of carbon. This should lead to a concentration of 40 a.p.p.m. in the sample. After being cold rolled, the ingot was homogenised at 1073 K for 24 h under high vacuum ($\approx 10^{-7}$ mbar) and air quenched (−16 °C/s). The thermal ageing, realised in quartz tubes under secondary vacuum ($\approx 10^{-7}$ mbar), were performed at 773 K for 50, 100, 150, 240 and 480 h. Two additional treatments (812 h and 1067 h at 773 K under primary vacuum ($\approx 10^{-5}$ mbar)) were realised afterward. For each condition, a 12 × 12 × 0.5 mm^3 sample was thermally aged.

* Corresponding author. Tel.: +33 23 2955131; fax: +33 23 2955932.
E-mail address: cristelle.pareige@univ-rouen.fr (C. Pareige).

0022-3115/$ - see front matter © 2008 Elsevier B.V. All rights reserved.
doi:10.1016/j.jnucmat.2008.10.008

2.2. Experimental technique

For all samples an Energy Compensated Tomographic Atom Probe (EC-TAP) with an aDLD detector was used [5]. The presence of an energy compensated lens [6] provides a high quality mass resolution of the mass spectra and the aDLD detector minimises the lost of information due to impact superposition or multi-event detection [5]. The basic principle of this technique may be found in different books or reviews [7]. The experimental conditions were carefully chosen in order to obtain accurate measurements especially phase composition. The FeCr system is known to be subjected: (i) to the so called local magnification effect that may affects the shape of precipitates during Atom Probe experiment and to (ii) the preferential evaporation of one chemical specie giving thus wrong chemical composition of phases. If nothing might be experimentally done to avoid the first effect (except afterward data treatments), care is needed during experiments to get accurate composition measurements. Thus the specimen was cooled down to a temperature of 40 K in order to mitigate the preferential field evaporation process of chromium atoms. A pulse repetition rate of 2000 Hz was used in order to prevent large multi-heat events on the detector. The atom probe specimen was electrically pulsed with a pulse fraction of 20%. The treatment of the data is performed using standard tools for Atom Probe characterisation [7]. As far as the measure of the composition and the evaluation of the size of the precipitates are concerned, a data filter in composition has been used. Indeed, it is necessary to isolate precipitates from the surrounding matrix. The Cr level of the matrix ranges between 20 and 14 at.%. Thus, a threshold of 40 at.% has been chosen in order to avoid counting atoms from the matrix. This value is calculated around each atoms of the analysed volume in a sampling sphere of 1 nm in diameter. When precipitates are thus defined, their core composition is measured with an adapted sampling volume. All the compositions reported in this work are quoted in atomic percent.

3. Results

At first, the as-quenched material (1073 K during 24 h and air quenched) was investigated in order to check and test the randomness of the spatial distribution of chromium atoms and to measure the exact solute concentration before any ageing at 773 K. The measured chromium concentration in the overall analysed volume is: 20.6 ± 0.2 at.%. The uncertainty on the composition is given by two standard deviation ($2\sigma = 2 \times (C(1-C)/N)^{1/2}$) where C is the atomic concentration and N the number of collected atoms). As it is clearly shown with the 3D distribution map of chromium atoms, on Fig. 1A, the 20.6% of chromium are homogeneously distributed, no particular segregation is observed before the ageing at 773 K. This is confirmed, even at fine scale, with the statistical χ^2 test comparing the two chromium distributions (experimental and binomial, Fig. 1B).

The 3D distributions of Cr atoms after the different ageing times (50, 100, 150, 240, 480, 812 and 1067 h) are shown in Fig. 2. In these conditions, nanometer-sized Cr-enriched precipitates are formed. The α/α' decomposition occurs, clearly revealed on Fig. 2 by the presence of chromium-enriched precipitates.

Characteristics of the α' precipitates are easily obtained taking into account and correcting the artefact linked to the field evaporation process. An accurate value of the size (radius) and volume fraction are thus achieved. Indeed as in the case of the largely studied Cu precipitation in the FeCu system [8], the chromium-rich phase is submitted to the local magnification effect. This effect is due to the difference of electrical field required for the evaporation of different phases (with different composition) [7]. It gives rise to

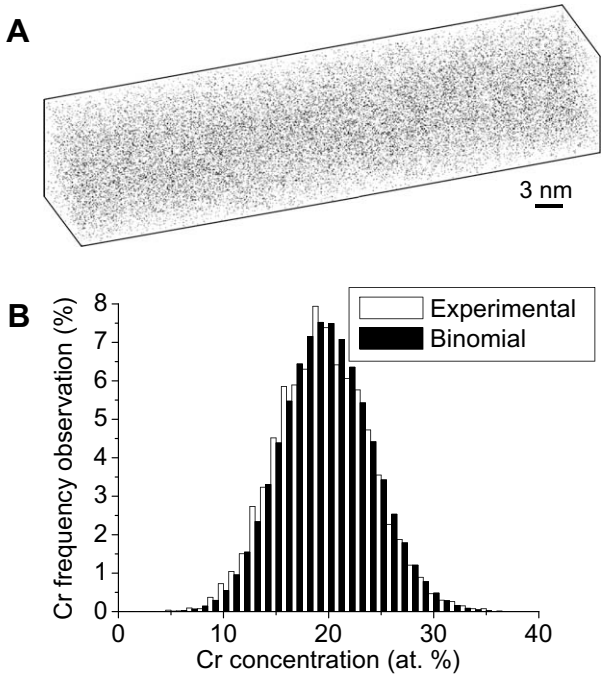

Fig. 1. (A) 3D distribution of chromium atoms in the material homogenized 24 h at 1073 K ($V = 10 \times 10 \times 50$ nm^3). Each dot represents one atom. For clarity only chromium atoms are represented. Chromium atoms are homogeneously distributed before aging. (B) Cr-concentration frequency distribution in the as-quenched material. The experimental distribution (white) is compared to the binomial one (black). The experimental distribution is obtained with sampling boxes of 100 atoms. Cr atoms are randomly distributed in the volume.

a compression of the phase with a low field of evaporation (α' precipitates in our case) in the x and y directions of analyses (i.e., the section perpendicular to the direction of analysis). However, this does not affect the particle characteristic in the *z-direction.* A sphere is thus becoming an ellipse. As it can be observed on Fig. 2, most of the particles look like ellipses rather than spheres (Fig. 2c–g) after 150 h of ageing. The reason for this will be given later. If the local magnification effect affect the shape of the α' precipitates, it has been shown by Blavette et al. [8], that it should have only a minor effect on the measured composition. Less than two percent of solvant (Fe in our case) may be introduced at the interface of the solute-rich particles.

The difference of field of evaporation induces another well known effect, the preferential evaporation of Cr atoms, that may introduces errors in the evaluation of the Cr-concentration. Owing to the experimental conditions of analyses, described above, this effect may lower the Cr-concentration of the α' phase of less than 1 at.%. This artefact is only observed for high-chromium concentration particles (see after) and the concentrations given in this work have been corrected.

The mean radii of the precipitates in all ageing condition are reported in Table 1. They have been averaged over a minimum of 80 particles and up to 240. The radius of each individual particle has been deduced from its number of atoms (n) ($R = \sqrt{\frac{3nV_{at}}{4\pi Q}}$ where $Q = 0.5$ is the efficiency of the atom probe detector; $V_{at} = a^3/2$ is the atomic volume with a the lattice parameter). It must be noted that the size of the precipitates obtained corresponds to the size deduced from the number of atomic planes detected along the direction of analysis in the case of an atomic plane by atomic plane experiment. This is illustrated on Fig. 3, where the 3D reconstruction shows an atomic plane by atomic plane reconstruction of a particle analysed along the ⟨1 1 0⟩ crystallographic direction of

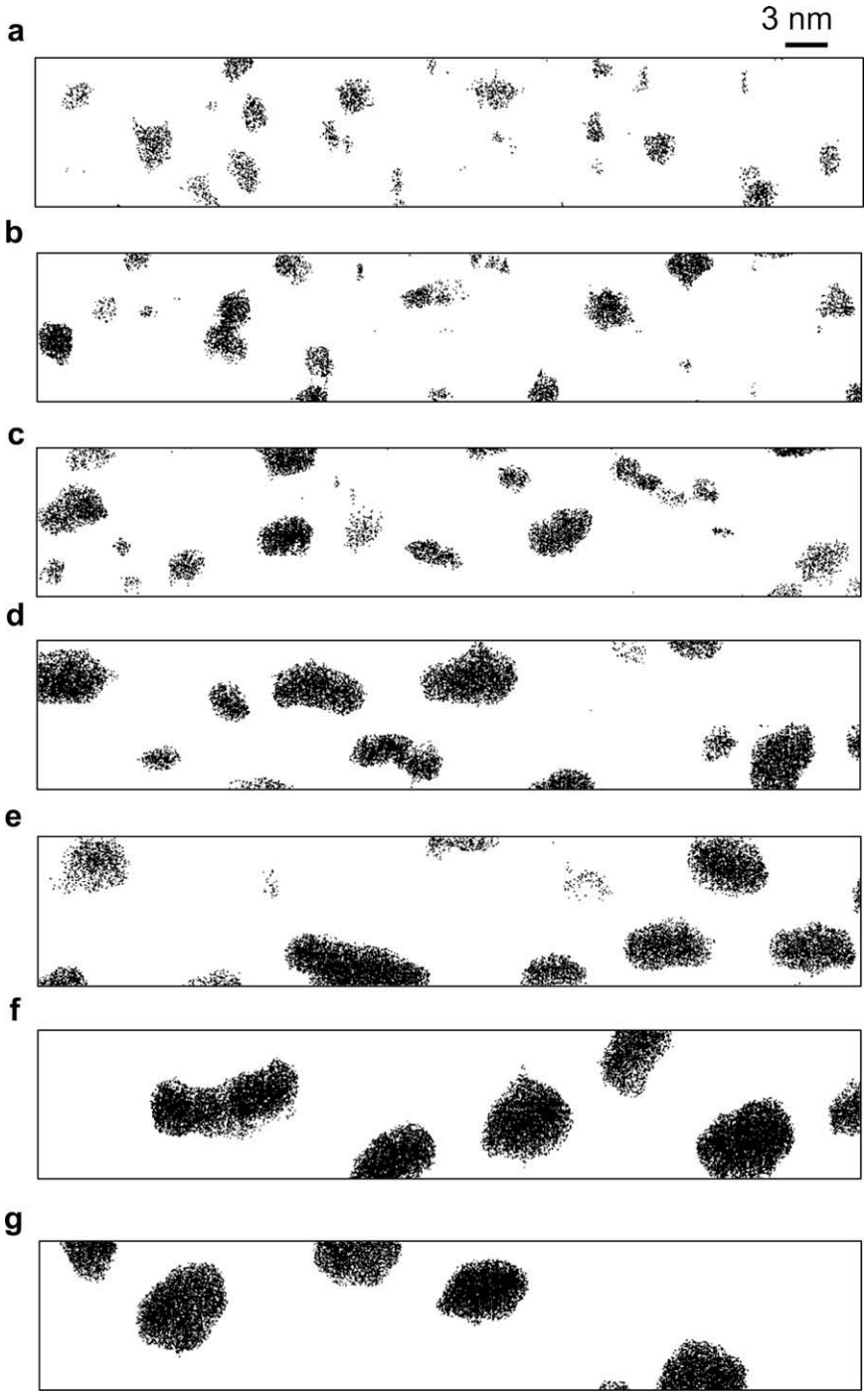

Fig. 2. Distribution of chromium-enriched precipitates in an Fe–20 at.%Cr after aging at 773 K for (a) 50 h, (b) 100 h, (c) 150 h, (d) 240 h, (e) 480 h, (f) 812 and (g) 1067 h ($V = 9 \times 9 \times 50$ nm^3). In all images the data are treated: only Cr-rich region where the local concentration is as high as 40 at.% are displayed.

Table 1
Mean radius of α' precipitates as function of ageing time in a Fe–20at.%Cr alloy at 773 K. The error represents the standard deviation from the mean value.

t (h)	Precipitate radius (nm)
50	0.95 ± 0.31
100	1.20 ± 0.33
150	1.40 ± 0.37
240	1.63 ± 0.44
480	1.96 ± 0.50
812	2.31 ± 0.74
1067	2.53 ± 0.51

the α-matrix in a material aged 150 h at 773 K. Fifteen atomic planes, separated by only $d_{\langle 110\rangle} = 0.21$ nm, are clearly reconstructed in the particle. This leads to a particle radius (along the analysis direction) of 1.47 nm which is in excellent agreement with the equivalent radius of 1.45 nm deduced from the number of atoms attributed to the precipitate.

In addition to this, a particular attention has been paid to the presence of coagulating precipitates. Precipitates interconnected by necks are visible on 3D images (Fig. 4). During ageing, the form of these coagulated precipitates pass trough interconnected form to elongated shape before reaching a spherical shape. These

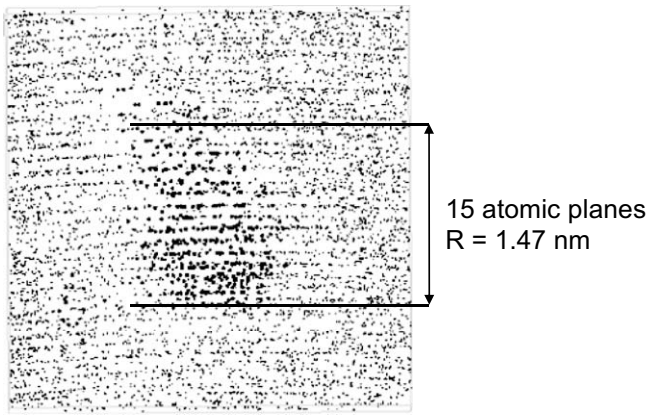

Fig. 3. Atomic plane by atomic plane analysis of a chromium-rich precipitate in an Fe–20 at.%Cr aged 150 h at 773 K. The straight lines are representative of the (1 1 0) planes. The interatomic distance in the [1 1 0] direction is 0.21 nm. The particle is formed of 13 atomic planes, indicating a radius of 1.13 nm. The smaller lateral size is due to the local magnification effect (compression along *x*- and *y*-direction). The overall volume of the figure is $V = 10 \times 3 \times 10\ \mathrm{nm}^3$. Chromium atoms are represented in black with a radius two times bigger than iron atoms.

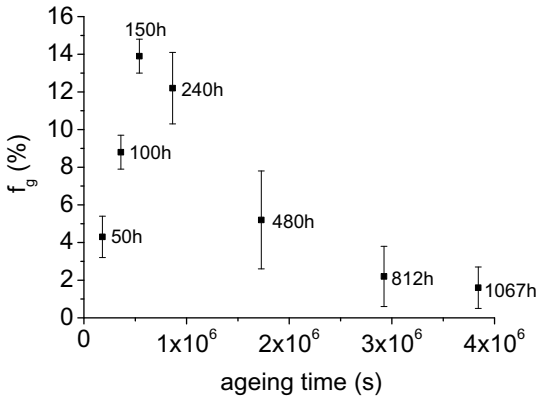

Fig. 5. Temporal evolution of the fraction (f_g) of coagulating α' precipitates in a Fe–20 at.%Cr at 773 K. f_g is defined as the simple ratio of the number of observed coagulating particles over the total number of particles in the analysed volume.

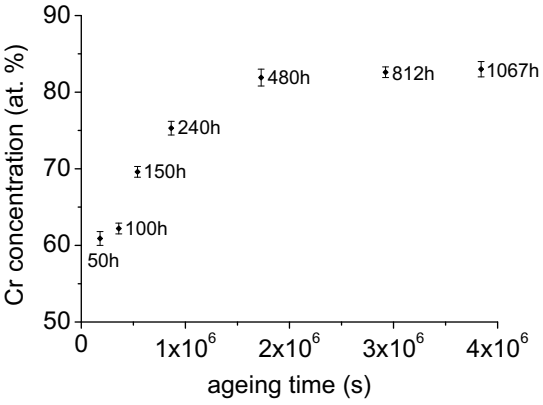

Fig. 6. Temporal evolution of the Cr-concentration of the α' phase in a Fe–20at.%Cr at 773 K.

elongated precipitates are in any direction of the volume. The randomness of the spatial distribution of these "long" precipitates is in favour of the presence of coagulating precipitates instead of artificially deformed precipitates (experimental artefact due to local magnification effect).

After 50 h of ageing, the fraction of coagulating precipitates (f_g: defined as the ration of coagulating precipitates over the total number of precipitates) is 4.3%. The maximum value of f_g, 13.9%, occurs after 150 h. Fig. 5 followed by a rapid decrease down to 2% after 812 h and 1.6% after 1067 h.

The Cr-concentration of the α' phase, for the different ageing time, is presented Fig. 6. This result reveals that the composition of precipitates evolves temporally from (60.6 ± 0.9) at.% after 50 h up to (83 ± 1) at.% after 1067 h. An asymptotic behaviour is observed at long ageing time. These results are in good agreement with the α' Cr-concentration determined by Kuwano [9] (85 at.%) and Dubiel and Inden [10] (88 ± 1) at.%. The difference between the results may be attributed to the too short ageing time and the slow kinetic of phase separation in this system. The results of Dubiel and Inden have been obtained on samples aged for 4 years and Kuwano's one on samples aged more than 2000 h.

In order to ensure that the progressive chromium-enrichment of the precipitates is not an experimental artefact (due to the local magnification effect (even if it has been shown that its contribution is small [8])), the correlation between the Cr-concentration and the precipitate radius has been studied. The graph, Fig. 7, shows the chromium concentration of each precipitate versus its size for 50 h and 1067 h of ageing. It appears that, for a given size (about 1.6 nm), after 1067 h of ageing precipitates have a Cr-concentration of at least 75 at.% (and up to 90 at.%), while after 50 h of ageing, the Cr-content is less than 70 at.%. This clearly shows that there is no correlation between the size of precipitates and their Cr-concentration. The Cr-content is only time dependant.

Moreover, it must be noted that precipitates detected after 50 h of ageing are spherical on the 3D reconstruction (i.e. without local magnification effect Fig. 2a), both spherical and ellipsoidal are observed after 150 h (Fig. 2c) and only ellipsoidal after 480 h (Fig. 2d–f). This observation is in favour of an increase of the Cr-content of the precipitates. The local magnification effect, due

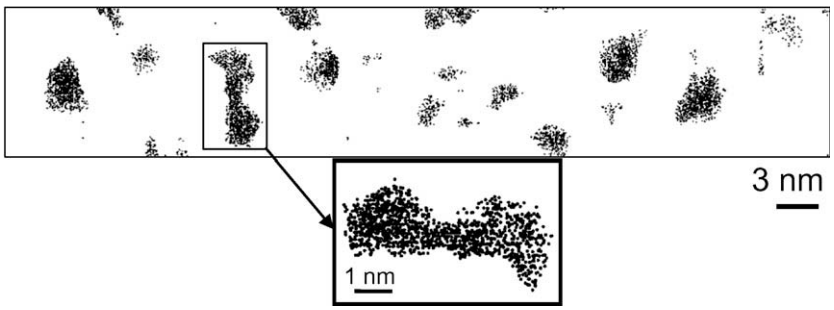

Fig. 4. Distribution of chromium-enriched precipitates in an Fe–20 at.%Cr after aging at 773 K for 100 h ($V = 9 \times 9 \times 50\ \mathrm{nm}^3$). Zoom of a coagulating precipitates. In all images the data are treated: only Cr-rich region where the local concentration is as high as 40 at.% are displayed.

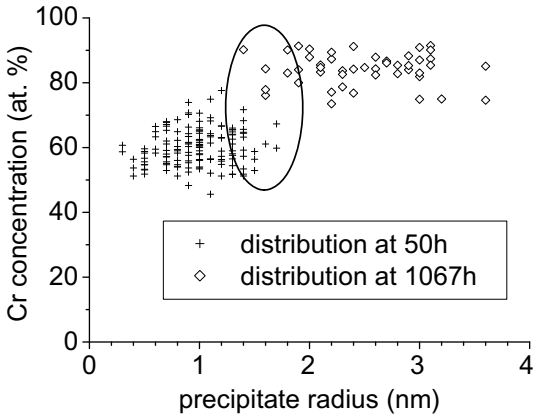

Fig. 7. Cr-concentration in α' precipitates as a function of their radii for 50 h and 1067 h of ageing in a Fe–20at.%Cr at 773 K. The marked area shows that precipitates with similar size (about 1.6 nm in radius) exhibit different chromium concentration.

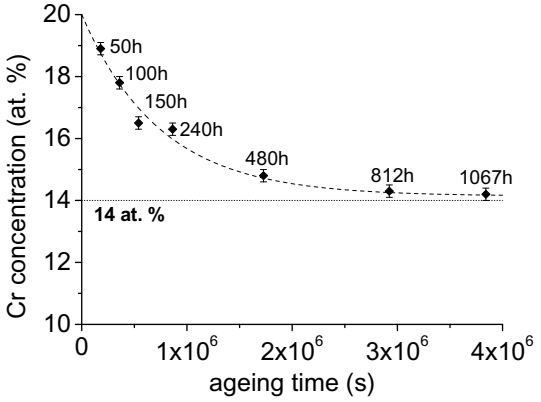

Fig. 8. Evolution of the Cr-concentration of the α phase with ageing time in a Fe–20 at.%Cr at 773 K. The horizontal line represents the lower chromium solubility limit measured by Dubiel and Inden [9].

to the difference between the Cr and Fe fields of evaporation, only appears when the Cr-content of the precipitate is high enough to significantly decrease the field of evaporation of the α' phase.

Fig. 8 shows the temporal evolution of the Cr-concentration of the α-matrix. An asymptotic value of 14 at.% is reach for the longer

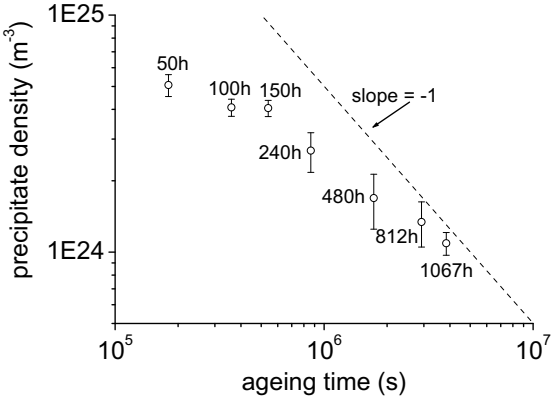

Fig. 9. Ln–ln plot of the number density of α' precipitates with ageing time in a Fe–20 at.%Cr at 773 K. The dashed line represents the t^{-1} law predicted for long ageing time.

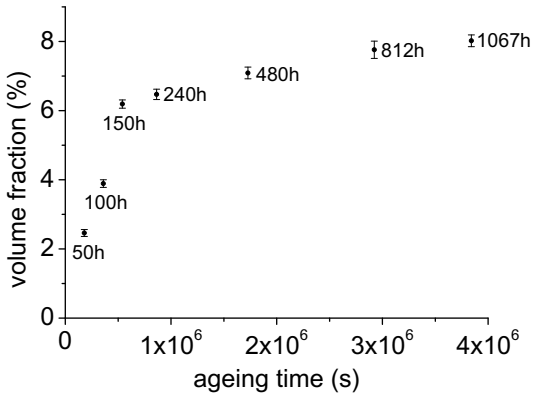

Fig. 10. Temporal evolution of the volume fraction of α' precipitates in a Fe–20 at.%Cr at 773 K.

ageing times. The Cr-equilibrium concentration of the α phase, as measured by Dubiel and Inden [10] at 773 K, ranges between 14 at.% (analysing a Fe–20.8 at.%Cr) and 16.5 at.% (analysing of a Fe–70.6 at.%Cr). These values are coherent with the results of Miller et al. [11] which show, by field ion microscopy, that no α'-precipitation is observed in a Fe–14 at.%Cr whereas ($\alpha + \alpha'$) phase separation occurs in a Fe–17 at.%Cr. According to all these results, the solubility limit of 11 at.% found by Kuwano [9] is too low. The solubility limit of chromium in the alpha phase at 773 K in the binary FeCr model alloy is close to 14 at.%.

The evolution of both the number density and the volume fraction of α' precipitates with time are shown Figs. 9 and 10. The number density was determined by a simple ratio of the number of the observed precipitates to the overall analysed volume. The volume fraction was defined as the ratio of the number of atoms contained inside the precipitates to the total number of atoms collected.

4. Discussion

It is well known that the theoretical description of the classical nucleation requires the nucleus composition to be uniform and almost equal to the equilibrium composition of the precipitating phase. This regime is also supposed to be observed only when the nominal concentration of the solute is close to the solubility limit. When the supersaturation increases, Cahn and Hillard [12–14] have shown that properties of the critical nucleus change: the interphase–interface becomes more diffuse and the composition at the core of the nucleus decreases with respect to the

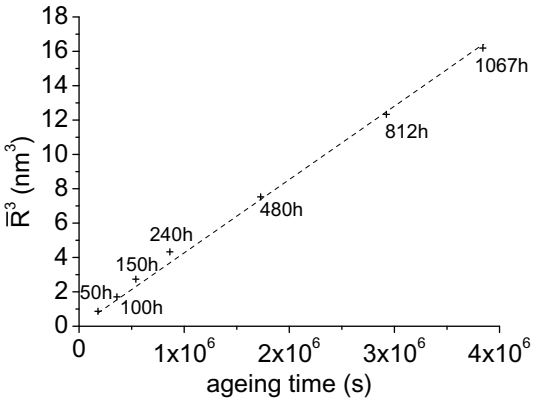

Fig. 11. Time dependence of the cube of the average precipitate radius.

equilibrium composition of the second phase. This work, and particularly the temporal evolution of the composition of the α' phase shown Fig. 6, clearly reveals that non-classical nucleation regime occurs in this alloy at $T = 773$ K.

Fig. 11 provides the quantitative time dependence of the averaged particle radius to the 3rd ($\bar{R}^3$). A linear behaviour of $\bar{R}^3$ is revealed as soon as 50 h of ageing indicating that the Cr diffusion is the rate-limiting step from 50 h of ageing. This is characteristic of the coarsening regime, the volume fraction not altering the time exponent predicted by the LSW (Lifshitz, Slyozov and Wagner) theory [15–16]. It must be noted that this result (evolution of $\bar{R}^3$) is in good agreement with previous works reported in the literature [17,18] from SANS experiments. As far as the radius and number density of particles is concerned a better agreement is found with reference [18]. A detailed comparison between our results and the SANS results is not reported here.

Because the coarsening regime is observed since 50 h of ageing, it is clear that the pure nucleation regime occurs before 50 h, in good agreement with the temporal evolution of the number density which does not show any increase (Fig. 9).

As far as the coarsening regime is concerned, even if it occurs from 50 h of ageing, it is worth noting that the time exponent of the temporal evolution of N_v (Fig. 9) evolves with time and tends toward the predicted -1 value only at long ageing time. This is not surprising since: (i) the volume fraction is very low at the beginning of the coarsening (only 2.7% at 50 h) and is still increasing with time (Fig. 10), (ii) the coagulation fraction is high (Fig. 5) and (iii) the equilibrium Cr-concentration of the α phase is not yet reached (Fig. 8). Within experimental errors, the equilibrium value of the solubility limit is only hardly reached after 1067 h of ageing and a non-zero fraction of coagulation is still observed. This indicates that the system is in a transient coarsening regime.

This transient coarsening regime is explained by an overlap between nucleation, growth and coarsening, as it has been proposed by Robson [19] with his modified version of the Kampmann and Wagner numerical precipitation model [20] based on the initial Langer–Schwartz model [21]. Indeed, if the initial supersaturation is large enough (it is, here, the case since a non-classical nucleation is observed as described above), a significant nucleation rate is retained even when a substantial proportion of the solute have been removed from the matrix, thus leading to an increase of the critical particle size. This critical size entering in the particle size distribution, all particles with a size under this critical value are dissolved. Then, whereas some α' precipitates are yet appearing, coarsening is already dissolving the smallest particles leading to a reduction in number density. This is coherent with the present experimental results since after 50 h the Cr-concentration of the solid solution is still close to the nominal one (18.9 at.%) offering the possibility to nucleation to occur.

The evolution of the particle size distribution (PSD) also clearly points out that a non-steady-state of coarsening occurs up to 1067 h as shown Fig. 12. It is found that the PSD passes through a continuous range of form. The narrow distribution observed after 50 h get wider to finally become bimodal after 812 h. At 1067 h, a narrowing of the distribution is observed to give again a monomodal PSD. The observed PSDs are quasi-symmetrical and not self-similar in this studied kinetic. This sequence of PSD's form has been shown to occurs, by Marder [22], when long-time correlations between precipitates develop. The study of this effect is in progress.

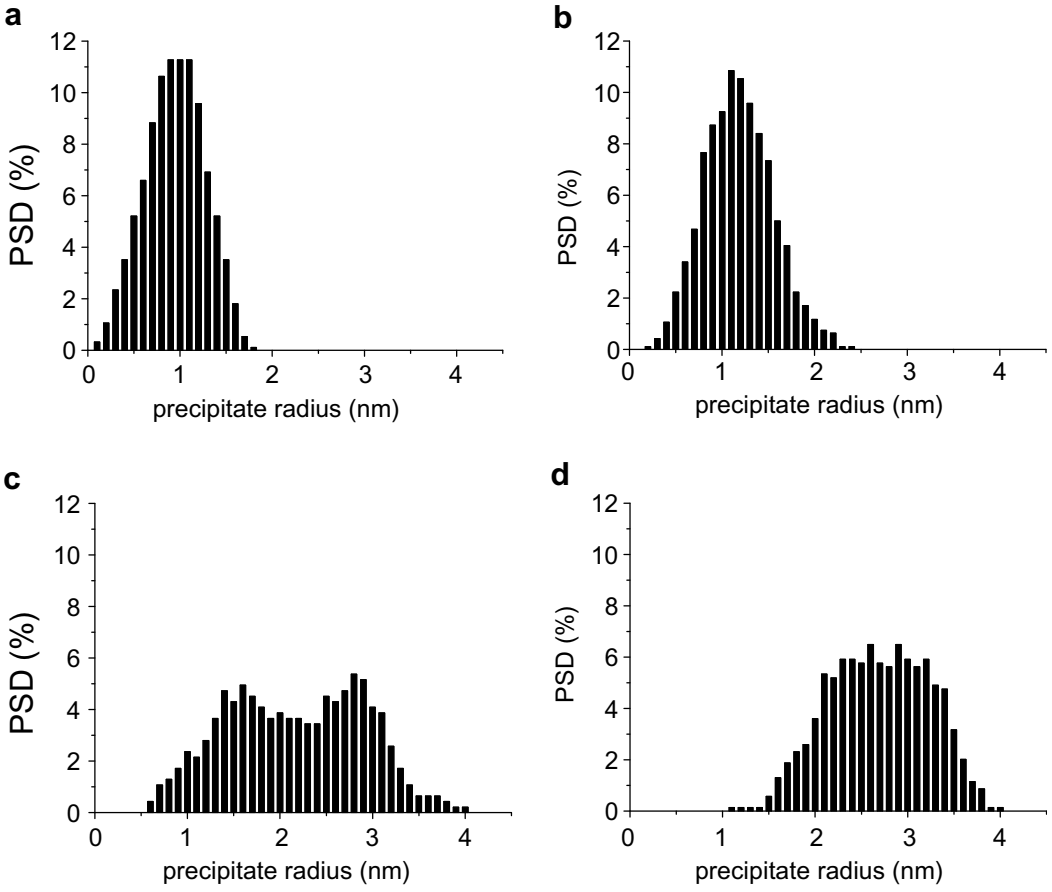

Fig. 12. Particle size distributions after: (a) 50 h, (b) 150 h, (c) 812 h, and (d) 1067 h of ageing in a Fe–20 at.%Cr aged at 773 K.

5. Conclusion

A quantitative study of the phase separation in a Fe–20at.%Cr aged at 773 K has been performed using the Tomographic Atom Probe. This work has shown that the chromium content in the α' phase evolves with ageing time in agreement with a non-classical nucleation mechanism. A linear evolution of the cube of the mean particle radius is observed from 50 h of ageing whereas the volume fraction of the second phase is still low. A transient coarsening regime is observed because of the overlap of the nucleation, growth and coarsening regimes. The steady-state of coarsening has not been observed in this work. The time evolution of the particle size distribution, fraction of coagulating precipitates, chemical composition of the α phase, volume fraction and number density of the α' phase show that a non-steady coarsening regime occurs before 1067 h. Also the time evolution of the measured Cr-concentration in the matrix tends toward an asymptotic value at 14 at.%, considered here as the solubility limit at 773 K. A maximum concentration of (83 ± 1) at.% is observed for the Cr-concentration in α' precipitates. These later values are in good agreement with previous published results.

Acknowledgements

This work has been performed under an EDF/CNRS research program. The materials were provided by Dr. A. Barbu (CEA-Saclay).

References

[1] M.Yu. Duc Nguyen-Manh, Sergei L. Lavrentiev, C.R. Dudarev, Physique 9 (2008) 379.
[2] G. Bonny, D. Terentyev, L. Malerba, Comput. Mater. Sci. 42 (2008) 107.
[3] P. Olsson, I.A. Abrikosov, J. Wallenius, Phys. Rev. B73 (2006) 104416.
[4] J. Wallenius, P. Olsson, L. Malerba, D. Terentyev, Nucl. Instr. Meth. Phys. Res. B255 (2007) 68–74.
[5] G. Da Costa, F. Vurpillot, A. Bostel, M. Bouet, B. Deconihout, Rev. Sci. Instr. 76 (2005) 013304.
[6] E. Bémont, A. Bostel, M. Bouet, G. Da Costa, S. Chambreland, B. Deconihout, K. Hono, Ultramicroscopy 95 (2003) 231.
[7] M. Miller, A. Cerezo, M. Hetherington, G. Smith, Atom Probe Field Ion Microscopy, Oxford Science Publications, 1996.
[8] D. Blavette, F. Vurpillot, P. Pareige, A. Menand, Ultramicroscopy 89 (2001) 145.
[9] H. Kuwano, Trans. Tapan Inst. Metal 26 (1985) 473.
[10] S.M. Dubiel, Z. Metallkde 79 (1987) 544.
[11] M.K. Miller, J.M. Hyde, M.G. Hetherington, A. Cerezo, G.D.W. Smith, C.M. Elliott, Acta Metall. Mater. 43 (1995) 3385.
[12] J.W. Cahn, J.E. Hilliard, J. Chem. Phys. 28 (1958) 258.
[13] J.W. Cahn, J. Chem. Phys. 30 (1959) 1121.
[14] J.W. Cahn, J.E. Hilliard, J. Chem. Phys. 31 (1959) 688.
[15] M. Lifshitz, V.V. Slyosov, J. Phys. Chem. Solid 19 (1961) 35.
[16] C. Wagner, Z. Elektrochem. 65 (1961) 581.
[17] V. Jacquet, PhD Thesis, Ecole Polytechnique, France, March 2000.
[18] F. Bley, Acta Metall. Mater. 40 (1992) 1505.
[19] J.D. Robson, Acta Mater. 52 (2004) 4669.
[20] R. Kampmann, R. Wagner, in: P. Haasen, V. Gerold, R. Wagner, M.F. Ashby (Eds.), Decomposition of Alloys: The Early Stages, Pergamon, Oxford, 1984, p. 91.
[21] J.S. Langer, A.J. Schwartz, Phys. Rev. A 21 (1980) 948.
[22] M. Marder, Phys. Rev. Lett. 55 (1987) 2953.